

SPARSE RECONSTRUCTION-BASED BEAMPATTERN SYNTHESIS FOR MULTI-CARRIER FREQUENCY DIVERSE ARRAY ANTENNA

Jie Xiong, Wen-Qin Wang

School of Communication and Information Engineering,
University of Electronic Science and Technology of China, Chengdu

ABSTRACT

Frequency diverse array (FDA) antenna using uniform frequency increments produces a S-shaped range-angle-dependent transmit beampattern, which can provide more degrees of freedom (DOFs) to suppress the interferences with different ranges. However, the S-shaped beampattern is coupled in the range-angle dimension and consequently results in inaccurate target localizations. In this letter, we proposed a multi-carrier FDA scheme to generate a dot-shaped transmit beampattern. To further improve the range-angle resolution capability, the sparse reconstruction respective of compressive sensing is also adopted. Theoretical analysis and simulation results demonstrate that the proposed approach produces a decoupled high-resolution dot-shaped beampattern. Moreover, both single-dot and multi-dot shaped beampatterns can be synthesized in this way.

Index Terms— Beampattern synthesis, frequency diverse array, array antenna, sparse reconstruction, dot-shaped beampattern.

1. INTRODUCTION

Phased-array offers a directional gain, which can be utilized to detect weak targets in interesting directions while suppressing undesired interferences from other directions. However, phased-array has a limitation of that the beam steering is only dependent on the angle parameter. To produce range-dependent transmit beampattern, frequency diverse array (FDA) was proposed [1] by using a small frequency increment across the array elements [2]. FDA is different from traditional orthogonal frequency division multiplexing (OFDM) [3] and multiple-input multiple-output (MIMO) [4] [5]. OFDM uses orthogonal subcarriers, whereas non-orthogonal carriers are employed in FDA. Another similar concept is the time-modulation array [6], which is mainly attributed to the weightings of each element by on/off switching the array elements sequentially.

The standard FDA using linearly increasing frequency increments will yield a S-shaped range-angle beampattern. This

limits its applications for unambiguously estimating target parameters. To decouple the range-angle response of targets, a transmit subaperturing is designed in [7] to focus the transmit energy into a certain range-angle sector to locate the targets. In [8], a nonuniform linear array is applied in the FDA. However, the transmitter and receiver must be placed accurately. Another nonuniform linear array for FDA is attempted to suppress/locate range dependent interference/target in [9], but it requires relocation of the elements mechanically in time. Moreover, a patent discusses the range-dependent characteristics [10]. A full-wave simulation of frequency diverse array antenna using the finite-difference time-domain (FDTD) method is proposed in [11]. Multipath characteristics with FDA over a ground plane are analyzed in [12]. Particularly, a logarithmically increasing frequency offset for FDA (Log-FDA) is proposed in [13] to decouple the range-angle beampattern, but it achieves poor resolution in both range and angle dimension. We also proposed a convex-multi-log-FDA (CML-FDA) in [14], which outperforms the Log-FDA, but the resolution is still need to be improved.

In this letter, we proposed a new multi-carrier FDA scheme to synthesize a dot-shaped high-resolution beampattern, and a sparse reconstruction based method is also proposed for the problem, which is solved with convex optimization tools. The rest of this letter is organized as follows. Section II gives the multi-carrier FDA model and proposes the sparse reconstruction based method for dot-shaped transmit beampattern synthesis. Numerical results and comparisons are provided in Section III and conclusions are drawn in Section IV.

2. MULTI-CARRIER FDA ANTENNA

2.1. System Description

Consider a multi-carrier FDA with uniform spacing d , as shown in Figure 1 with θ being the azimuth angle. The m th carrier frequency of the n th array element is

$$f_{n,m} = f_0 + m\Delta f_n, \quad -N \leq n \leq N, 0 \leq m \leq M \quad (1)$$

where f_0 is the frequency for the first carrier of the first element, $M + 1$ and $2N + 1$ denote the number of carriers trans-

This work was supported by National Natural Science Foundation of China under grant61571081.

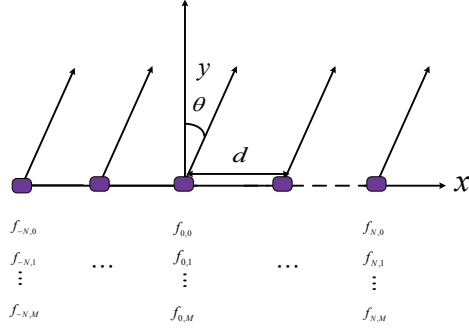


Fig. 1. The proposed multi-carrier FDA system model

mitted by each antenna and the number of array elements, respectively. The frequency offset Δf_n is determined by

$$\Delta f_n = \Delta f \log(|n| + 1), \quad -N \leq n \leq N \quad (2)$$

with $\Delta f \ll f_0$ being the fixed frequency increment.

Since we consider primarily beam pattern synthesis, the signal transmitted at the carrier frequency $f_{n,m}$ can be simply expressed as

$$x_{n,m}(t) = w_{n,m} a_{n,m}, \quad -N \leq n \leq N, \quad 0 \leq m \leq M \quad (3)$$

where $w_{n,m}$ is the complex weight associated with $f_{n,m}$ and $a_{n,m} = e^{j2\pi f_{n,m}(t - \frac{R_n}{c})}$ with R_n being the distance from the target to the n th array element and c the speed of light. Under the far-field assumption, the R_n can be approximated as $R_n \approx R - nd \sin \theta$.

The signals arrived at the position (R, θ) can be expressed as

$$\begin{aligned} X(t; R, \theta) &= \sum_{n=-N}^N \sum_{m=0}^M x_{n,m}(t) \\ &= \sum_{n=-N}^N \sum_{m=0}^M w_{n,m} e^{j2\pi f_{n,m}(t - \frac{R - nd \sin \theta}{c})} \end{aligned} \quad (4)$$

Substituting (1) and (2) into (4) yields

$$\begin{aligned} X(t; R, \theta) &= \sum_{n=-N}^N \sum_{m=0}^M w_{n,m} e^{j2\pi(f_0 + m\Delta f \log(|n|+1))(t - \frac{R - nd \sin \theta}{c})} \end{aligned} \quad (5)$$

Correspondingly, the array factor (AF)[7] is

$$\begin{aligned} \text{AF}(t; R, \theta) &= \left| \sum_{n=-N}^N \sum_{m=0}^M w_{n,m} e^{j2\pi f_0 \frac{nd \sin \theta}{c}} e^{j2\pi m \Delta f \log(|n|+1)(t - \frac{R}{c})} \right| \end{aligned} \quad (6)$$

2.2. Sparse Reconstruction-Based Beam pattern Synthesis

For notation convenience, we adopt vector form by defining

$$\mathbf{A} = \begin{bmatrix} a_{-N,0} & \cdots & a_{0,0} & \cdots & a_{N,0} \\ a_{-N,1} & \cdots & a_{0,1} & \cdots & a_{N,1} \\ \vdots & \vdots & \vdots & \vdots & \vdots \\ a_{-N,M-1} & \cdots & a_{0,M-1} & \cdots & a_{N,M-1} \\ a_{-N,M} & \cdots & a_{0,M} & \cdots & a_{N,M} \end{bmatrix} \quad (7)$$

and

$$\mathbf{W} = \begin{bmatrix} w_{-N,0} & \cdots & w_{0,0} & \cdots & w_{N,0} \\ w_{-N,1} & \cdots & w_{0,1} & \cdots & w_{N,1} \\ \vdots & \vdots & \vdots & \vdots & \vdots \\ w_{-N,M-1} & \cdots & w_{0,M-1} & \cdots & w_{N,M-1} \\ w_{-N,M} & \cdots & w_{0,M} & \cdots & w_{N,M} \end{bmatrix} \quad (8)$$

where \mathbf{A} and \mathbf{W} denotes the $(2N + 1) \times (M + 1)$ steering matrix and weight matrix, respectively. Furthermore, by vectorizing these two matrices, we have

$$\begin{aligned} \mathbf{a} &= \text{vec}(\mathbf{A}) \\ &= \{a_{-N,0} \cdots a_{-N,M}, a_{-N+1,0} \cdots a_{-N+1,M} \cdots a_{N,0} \cdots a_{N,M}\} \end{aligned} \quad (9)$$

and

$$\begin{aligned} \mathbf{w} &= \text{vec}(\mathbf{W}) \\ &= \{w_{-N,0} \cdots w_{-N,M}, w_{-N+1,0} \cdots w_{-N+1,M} \cdots w_{N,0} \cdots w_{N,M}\}. \end{aligned} \quad (10)$$

The corresponding \mathbf{a} and \mathbf{w} can be regarded as the steering vector and weight vector, respectively.

To derive the second-order statistics of transmitted signal, let \mathbf{R}_z denote the theoretical covariance matrix of the transmitted signal, which is a positive definite matrix:

$$\mathbf{R}_z = \mathbf{a} \mathbf{a}^H = \sigma^2 \mathbf{a} \mathbf{a}^H \quad (11)$$

where the interested signal \mathbf{s} is assumed to be zero-mean uncorrelated gaussian processes. σ^2 is the powers of the uncorrelated impinging signal, $(\cdot)^H$ is the conjugate transpose operator.

The dot-shape transmit beam pattern synthesis can be formulated as optimal design of the weighting vector \mathbf{w} . Firstly, we make the following definitions: $\mathbf{a}(R_0, \theta_0)$ is the steering vector at the target location (R_0, θ_0) and $\mathbf{a}(R_s, \theta_s)$ denotes the sidelobe area, respectively. For notation convenience, we define

$$\Pi = (R_0, \theta_0) \quad (12)$$

and

$$\Theta_i = (R_s^i, \theta_s^i) \quad (13)$$

where i denotes the i th sidelobe.

The sparse constraint encourages sparse distribution for $\mathbf{G} = [\mathbf{a}^H(\theta_1), \mathbf{a}^H(\theta_2), \dots, \mathbf{a}^H(\theta_L), \dots, \mathbf{a}^H(\theta_L)]$ with a fixed spacing, where L is the number of grids for the array configuration and \mathbf{G} denotes all the array gains. Actually, the array gains in the mainlobe are not sparse and thus, the l_1 norm minimization based sparse constraint is applied only in the sidelobe region $\mathbf{G}_\Theta = [\mathbf{a}^H(\theta_1), \mathbf{a}^H(\theta_2), \dots, \mathbf{a}^H(\theta_{s-B}), \mathbf{a}^H(\theta_{s+B}), \dots, \mathbf{a}^H(\theta_L)]$, with B is an integer associated with the bounds between the beampattern mainlobe and sidelobe. To further improve the beamforming performance, the l_∞ norm minimization is also imposed on the sidelobes \mathbf{G}_Θ . In doing so, the proposed sparse reconstruction based constraint beamformer optimization can be recast as

$$\begin{aligned} \min_{\mathbf{w}} \quad & \mathbf{w}^H \mathbf{R}_z \mathbf{w} + \eta \|\mathbf{w}^H \mathbf{G}_\Theta\|_1 \\ \text{s. t.} \quad & \|\mathbf{w}^H \mathbf{G}_\Pi - 1\|_\infty \leq \varepsilon \\ & \|\mathbf{w}^H \mathbf{G}_\Theta\|_\infty \leq \varepsilon \end{aligned} \quad (14)$$

where η is the weighting factor to balance the minimum variance constraint between the total energy and sparse constraint on the sidelobe, and the parameter ε determines the array performance. The product $\mathbf{w}^H \mathbf{G}_\Theta$ indicates the sidelobe gain, and the $\|\mathbf{w}^H \mathbf{G}_\Theta\|_1$ is imposed to suppress the sidelobe level. Finally, (14) can be easily solved by the open-accessed convex optimization tool CVX.

3. SIMULATION AND RESULTS

In this section, we suppose the following parameters for all the simulations: $d = \lambda_{\max}/2$, $f_0 = 10 \text{ GHz}$, $\Delta f = 2 \text{ kHz}$, $M = 7$, $N = 8$, and $\eta = 0.1$. For comparison purpose, standard FDA [1], Log-FDA [13] and CML-FDA [14] are also simulated with the same parameters.

3.1. Dot-Shaped Transmit Beampattern Synthesis

Suppose one desired direction at $(R_0, \theta_0) = (525 \text{ km}, 25^\circ)$, Figure 2 compares the proposed multi-carrier FDA with three existing FDAs. Our method produces a satisfactorily focused peak in the transmit beampattern, while the standard FDA generates unfocused and range-angle coupled peaks. Although the log-FDA and CML-FDA also generate dot-shaped beampattern, they have poor resolution performance both range and angle dimensions. This implies that the proposed can achieve better interference performance and higher signal-to-interference-plus-noise ratio (SINR) performance, as clearly shown in Figures 3 and 4. Particularly, Figure 2(b) shows the Log-FDA beampattern achieves poor resolution in both range and angle dimension.

3.2. PSR and Beam Width Analysis

To numerically show the results, Table I compares the peak-sidelobe ratio (PSR) performance of the proposed method

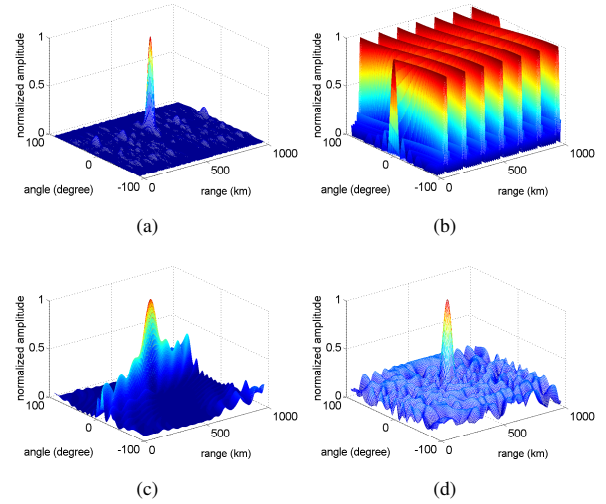


Fig. 2. Comparisons of synthesized transmit beampatterns for one desired direction: (a) Proposed multi-carrier FDA, (b) Standard FDA, (c) Log-FDA, (d) CML-FDA.

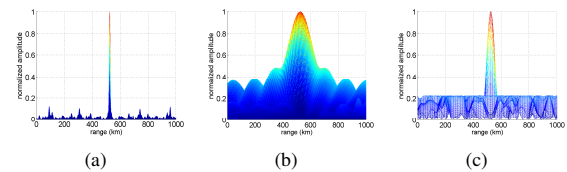


Fig. 3. Profile of transmit beampattern in range dimension: (a) Proposed multi-carrier FDA, (b) Log-FDA, (c) CML-FDA.

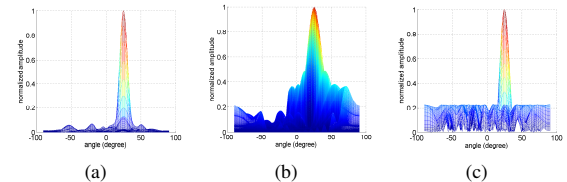


Fig. 4. Profile of transmit beampattern in angle dimension with: (a) Proposed multi-carrier FDA, (b) Log-FDA, (c) CML-FDA.

with existing Log-FDA method and CML-FDA. Their PSRs are 0.48, 0.23 and 0.11, respectively. This means that our proposed method has better PSR performance. Moreover, by comparing the scope of the beam width, our method has better resolution performance in both range and angle dimensions. That validates again that our proposed method has better range and angular resolution and accordingly, we can accomplish more precise control of the spatial scanning beam direction.

Table 1. Comparisons of PSR Results

$(R_0, \theta_0) = (525km, 25^\circ)$	Log-FDA [13]	CML-FDA [14]	our multi-carrier FDA
PSR	0.48	0.23	0.11
Range beam width (3dB)	412 km ~ 643 km	496 km ~ 557 km	516 km ~ 534 km
Angle beam width (3dB)	$13^\circ \sim 40^\circ$	$18^\circ \sim 32^\circ$	$20^\circ \sim 30^\circ$
Range beam width (6dB)	0 km ~ 1000 km	484 km ~ 561 km	510 km ~ 530 km
Angle beam width (6dB)	$-5^\circ \sim 69^\circ$	$16^\circ \sim 34^\circ$	$18^\circ \sim 32^\circ$

3.3. Multiple Dot-Shaped Transmit Beampattern Synthesis

We performed also multi-dot shaped beampattern synthesis simulations. Suppose there are two targets located at $(R_1, \theta_1) = (625km, -50^\circ)$ and $(R_2, \theta_2) = (325km, 40^\circ)$, respectively. Figure 5 (a) shows that two well focused peaks are synthesized at the desired target positions. Obviously, it outperforms both the log-FDA shown in Figure 5(b) and CML-FDA shown in Figure 5(c) in terms of range and angle resolution and PSR performance.

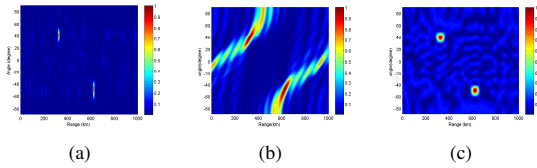


Fig. 5. Comparisons of two-dot shaped beampattern: (a) Proposed multi-carrier FDA, (b) Log-FDA, (c) CML-FDA.

4. CONCLUSION

This letter proposed a multi-carrier FDA with sparse reconstruction based method for dot-shaped transmit beampattern synthesis. Different from traditional methods, the proposed method decoupled the effect between range and angle dimension. Furthermore, the proposed FDA scheme outperforms the existing FDAs in at least three aspects: 1) generates a more focused dot-shaped beampattern with higher resolution in both range and angle dimensions; 2) much lower sidelobes in undesired area; 3) without ambiguous beampattern peaks, which can potentially be exploited for suppressing range-angle-dependent interferences.

5. REFERENCES

- [1] P. Antonik, M. C. Wicks, H. D. Griffiths, and C. J. Baker, Frequency diverse array radars, in *Proceedings of the IEEE Radar Conference*, Verona, NY, April 2006, pp. 215–217.
- [2] J. Huang, K. F. Tong, and C. J. Baker, “Frequency diverse array with beam scanning feature,” in *Proceedings of the IEEE Antennas and Propagation Conference*, San Diego, California, USA, Jul.2008, pp. 1–4.
- [3] S. Sen, “OFDM radar space-time adaptive processing by exploiting spatio-temporal sparsity,” *IEEE Transactions on Signal Processing*, vol. 61, no. 1, pp. 118–130, January 2013.
- [4] S. Ahmed and M.-S. Alouini, “MIMO-radar waveform covariance matrix for high SINR and low side-lobe levels,” *IEEE Transactions on Signal Processing*, vol. 62, no. 8, pp. 2056–2065, April 2014.
- [5] G. L. Cui, H. B. Li, and M. Rangaswamy, “MIMO radar waveform design with constant modulus and similarity constraints,” *IEEE Transactions on Signal Processing*, vol. 62, no. 2, pp. 343–353, January 2014.
- [6] K.-J. Koh and H. Elyas, “Time-interleaved phased arrays with parallel signal processing in RF modulation,” *IEEE Transactions on Antennas and Propagation*, vol. 62, no. 2, pp. 677–689, February 2014.
- [7] W.-Q. Wang, H. C. So. “Transmit subaperturing for range and angle estimation in frequency diverse array radar,” *IEEE Transactions Signal Processing*, vol. 62, no. 8, pp. 2000–2011, 2014.
- [8] P. F. Sannmartino, C. J. Baker, and H. D. Griffiths, “Frequency diverse MIMO techniques for radar” *IEEE Transactions on Aerospace and Electronic Systems*, vol. 49, no. 1, pp. 201–222, January 2013.
- [9] W.-Q. Wang, H. C. So, and H. Z. Shao, “Nonuniform frequency diverse array for range-angle imaging of targets” *IEEE Sensors Journal*, vol. 14, no. 8, pp. 2469–2476, August 2014.
- [10] M. C. Wicks and P. Antonik, “Method and apparatus for a frequency diverse array,” *US Patent 7511665B2*, March 31, 2009.
- [11] J. Shin, J.-H. Choi, J. Kim, J. Yang, W. Lee, J. So, and C. Cheon, “Full wave simulation of frequency diverse array antenna using the FDTD method,” *Asia-Pacific Microwave Conference Digest*, Seoul, November 5th, pp. 1070–1072, 2013.
- [12] C. Cetinepe and S. Demir, “Multipath characteristics of frequency diverse arrays over a ground plane,” *IEEE Transactions on Antennas and Propagation*, 10.1109, 2014.
- [13] W. Khan, I. M. Qureshi, and Sarah Saeed, “Frequency diverse array radar with logarithmically increasing frequency offset,” *IEEE antennas and wireless propagation letters*, vol. 14, pp. 499–502, 2015.
- [14] H. Z. Shao, J. Dai, J. Xiong, H. Chen, et al. “Dot-Shaped Range-Angle Beampattern Synthesis for Frequency Diverse Array,” *IEEE antennas and wireless propagation letters*, 1–1, 2016.